

# SEA ICE LEADS AND POLYNIA DETECTION USING MULTI-MISSION ALTIMETRY IN THE GREENLAND SEA

Felix L. Mueller, Marcello Passaro, Denise Dettmering and Wolfgang Bosch

*Deutsches Geodätisches Forschungsinstitut der Technischen Universität München (DGFI-TUM), Germany*

## ABSTRACT

In this study, we present two methods to detect open water areas in the Greenland Sea based on altimetry measurements. For this purpose, high-frequency data from ENVISAT (pulse-limited altimeter) and Delay-Doppler data from CryoSat-2 are used. The radar echoes of both missions contain information about the reflectance of the overflown surface area. For ENVISAT, we use an unsupervised classification approach to distinguish between water and ice returns. The waveforms are the main input for the classification process. Training data from known surfaces are not necessary for our method. For CryoSat-2 SAR mode, an advanced approach is used in order to exploit the multi-look processing of the same resolution cell from different look angles. We analyse the Range Integrated Power, a side product providing additional information about the backscatter properties. All classification results are compared with pictures of imaging SAR satellite missions (ALOS and Sentinel-1A). In order to take the time lag between the two observation sets into account, a mean ice-motion is applied to the images. This ensures realistic comparison results. The classification approach allows for an identification of open water (leads and polynyas) in sea-ice regions and will help to improve sea level estimation in these regions.

Key words: waveform; unsupervised classification; Delay-Doppler; Range Integrated Power; peakiness.

## 1. INTRODUCTION

In order to use satellite altimetry data to estimate sea surface heights and ocean flows in the Greenland Sea it is necessary to exclude unreliable observations contaminated by sea ice. For this purpose, open water regions (i.e. leads and polynyas) have to be detected. Sea ice leads are narrow and very straight-lined features up to tens of kilometers long. In contrast, polynyas are non-linear shaped regions enclosed by ice and appear often close to the coast or ice shelves.

The shape of the returning altimeter echoes (so-called waveforms) is strongly affected by the surface reflectance and characteristics. Smooth surfaces and calm water ar-

reas produce specular and peaky waveforms. In contrary, open ocean returns show wider waveforms and ice returns contain more peaks and are usually very noisy. In addition, different mission characteristics, e.g. different types of sensor and orbit, influence the size of the altimeter footprint. Moreover, the repetition frequency of the measurements as well as environmental circumstances e.g. various sea ice types have to be considered.

For conventional altimetry missions such as ENVISAT, an unsupervised classification without the use of any training data is performed in order to separate open water returns from sea ice returns. For Delay-Doppler altimetry data of CryoSat-2, the surface sample stack is used to detect open water. For this purpose, a threshold-based algorithm is applied based on the Range Integrated Power, i.e. the power contained in each look of a resolution cell. To evaluate the quality of our lead and polynya detection a comparison of the classification results with imaging SAR is performed.

## 2. CLASSIFICATION OF MULTI-MISSION ALTIMETRY DATA

In this section the different methods for lead and polynya detection are described. In the first part, the methodology of the unsupervised classification using ENVISAT waveforms are explained. The second part describes the method we use for the classification of Delay-Doppler data of CryoSat-2.

### 2.1. Unsupervised classification of conventional altimetry waveforms (ENVISAT)

The altimetry radar pulses show various shapes and characteristics depending on the reflecting surface. To assign each waveform to a specific surface class (classification), a classification model has to be created in a first step. To define the classes, we choose a set of different waveforms from the investigation area (one ENVISAT cycle) and group them automatically into different classes, a process called clustering. For this task, a K-medoids cluster algorithm [1] is implemented which categorizes the waveform based on different waveform features into a pre-defined

number of classes. However, it is challenging to select the optimal waveform features and to set an appropriate number of classes. In this study, we use 6 features (such as maximum power, peakiness, skewness etc.) and 20 classes. The created model is used to classify all remaining waveforms of the entire mission. This is done by a nearest-neighbor classification algorithm [2]. In Fig. 1 the flowchart of the unsupervised classification is shown.

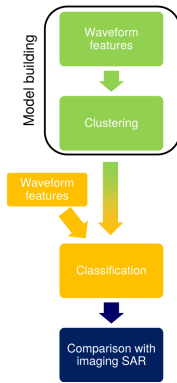


*Figure 1. Flowchart of processing steps of the unsupervised classification approach.*

The clustering result of K-medoids is shown in Fig. 2. The plot illustrates 20 classes of waveforms. For each cluster, the class number and the number of assigned waveforms is given. Class 5,8,9,15, and 20 represent very peaky waveforms and refer to lead or polynya returns. These classes are important for the following open water detection by a nearest-neighbor classification. The remaining classes typify ocean and radar pulses contaminated by sea ice.

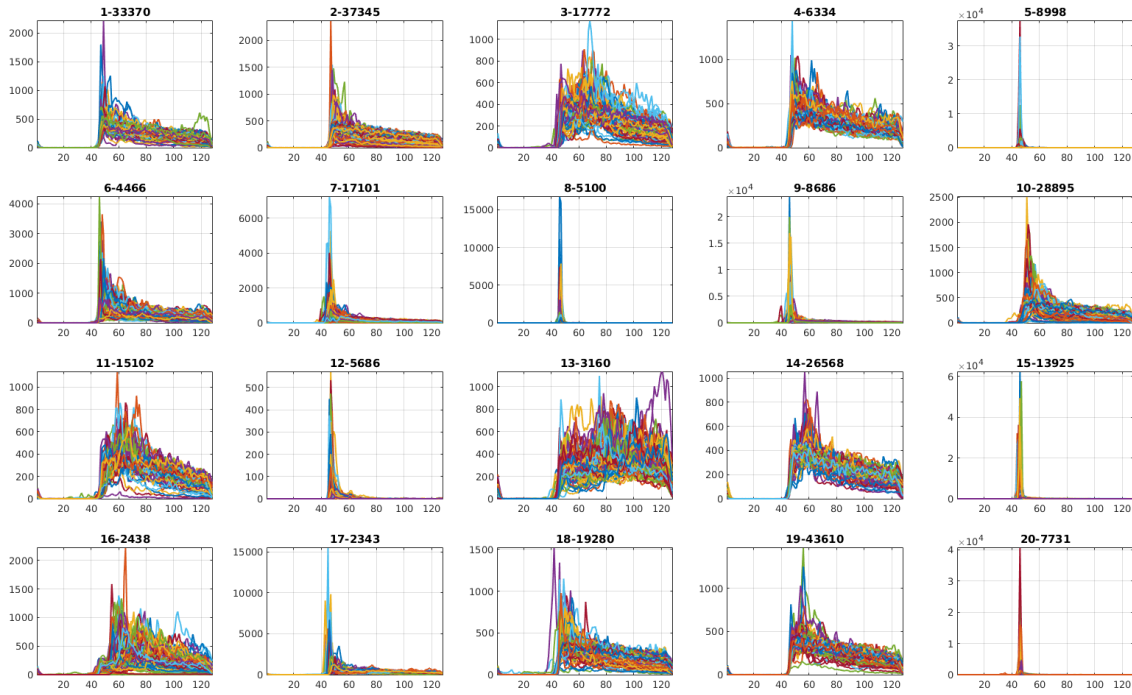


Figure 2. ENVISAT waveform classes after K-medoids clustering and number of test waveforms belonging to each class.

## 2.2. Threshold based classification of the Delay-Doppler altimetry waveforms (CryoSat-2)

By exploiting the Doppler effect, Delay-Doppler altimeters are able to perform multi-looked acquisitions, i.e. to associate to a resolution cell a certain number of looks (variable depending on the processing settings) acquired at different look angles as the satellite flies over the imaged area.

Using processing techniques inherited from the SAR processing, such as range compression and range migration correction, all the returns corresponding to the resolution cell are aligned in a stack diagram (Fig. 3A). The CryoSat-2 multilooked radar waveforms, such as the one in Fig. 3C, are obtained by summing in the along-track dimension all the single echoes in the stack. By summing up the returns in the cross-track dimension (Fig. 3B), the so-called stack waveform, or Range Integrated Power (RIP) waveform, can be generated. It contains information concerning the backscattering properties of the illuminated surface, but it also reveals details of the distribution of the scatterers as the satellite spans different look angles passing over the nadir position.

Generally speaking, when the satellite flies over a very smooth surface, as in the case of leads, the signal will be specularly reflected back and the stack waveform will be peaky. In contrast, when flying over areas containing scatterers with different orientation (e.g., wavy seas or ice) the backscattered power will rather be normally distributed.

The Delay-Doppler altimeter onboard CryoSat-2 provides new capabilities for lead detection. In particu-

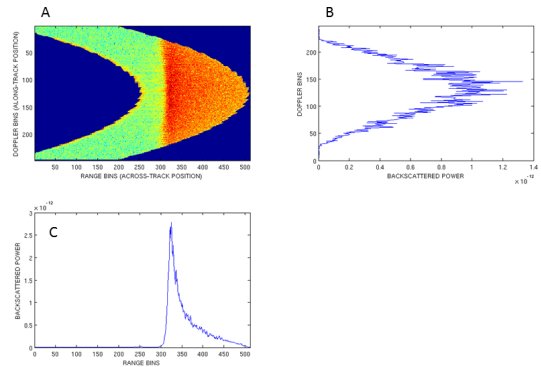


Figure 3. Example of a stack diagram (A), a stack waveform (B) and a multilooked waveform (C) acquired by CryoSat-2 over sea ice.

lar, the beam-limited along-track footprint size (roughly 300 m, [3]) should guarantee a more precise determination of the lead position. Nevertheless, due to the size of the pulse-limited across-track footprint (1.65 km), the distinction of a lead return at nadir from an off-nadir reflection is still challenging and previous studies have demonstrated how a lead-return can dominate the waveform despite being further away from the sub-satellite point [4].

The information coming from the stack enables us to compare the strength of the specular return registered by the satellite at zero look angle with the returns from the same beam seen from different angles. In order to ob-

serve the variation of the stack power along a track overflying the sea ice region, we define the Stack Peakiness  $PP_{stack}$ , computed on the RIP waveform normalised by the maximum value:

$$PP_{stack} = \frac{1}{\overline{P}_{l,r}} \quad (1)$$

where:

$$\overline{P}_{l,r} = \frac{\sum_{i=1}^N P(i)_{l,r}}{N} \quad (2)$$

$P(i)_{l,r}$  is the power from the look angle  $i$ , excluding the nadir look (i.e., at its right or left). In Fig. 4 the typical behaviour of the  $PP_{stack}$  is shown. The  $PP_{stack}$  has an almost constant value over ice, but peaks are clearly distinguishable. The peaks are not isolated, but they are preceded and followed by ascending and descending slopes of  $PP_{stack}$ . Therefore, it is possible to determine the position in which the return from the nadir look has the highest power in comparison with the other look angles. We argue that the local  $PP_{stack}$  maximum corresponds to the nadir location in which the lead crosses the altimeter track.

It is of course possible that a lead runs parallel to the altimeter track and never crosses it. In this case,  $PP_{stack}$  will still reach a peak, but  $PP_{stack}$  local maxima will be relatively smaller, given that the farther away is the lead from nadir the more power will be reflected away from the sensor [5]. From empirical experiments, we have set a minimum peak  $PP_{stack}$  threshold of 100: if the local maxima is below the threshold, the point will not be classified as lead.

The main novelties of our technique are the use of a new stack statistic (partially inherited from the right and left peakiness of the along-track waveform described in [6]) and the classification based on the evaluation of consecutive stacks rather than on single values.

The  $PP_{stack}$  is needed because the parameters given in the CryoSat-2 products and used up to now in previous studies are not sufficient to clearly compare the zero look angle view with the rest of the stack: The stack standard deviation parameter is based on a Gaussian fitting of the RIP, which is not efficient for peaky waveforms; The Kurtosis parameter is based on the mean over all the look angles and can be inefficient in particular in case of residual sidelobe effects that cause high power in the look angles different from zero.

Our solution, aimed at reducing the identification of off-nadir leads, is particularly suitable to identify the nadir returns from narrow and elongated specular features. Figure 5 shows a modelled example. Previous studies have shown how most of the leads are narrower than 1 km ([7], [8]), while being several km long. Considering the dimensions of the along-track footprint, such narrow leads cross the altimeter track in a single beam, which our method identifies.

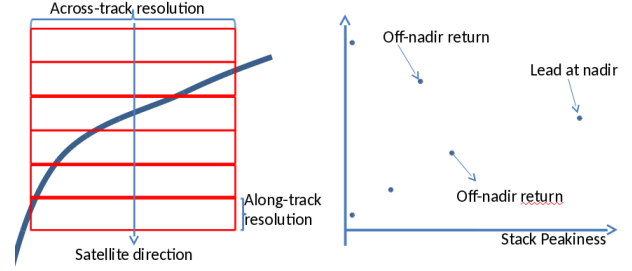


Figure 4. The modelled problem. An elongated narrow lead (in blue) crosses the satellite track and is seen at different cross-track locations from consecutive beams. This corresponds to increasing and decreasing values of Stack Peakiness ( $PP_{stack}$ ), with a maximum at the nadir crossing.

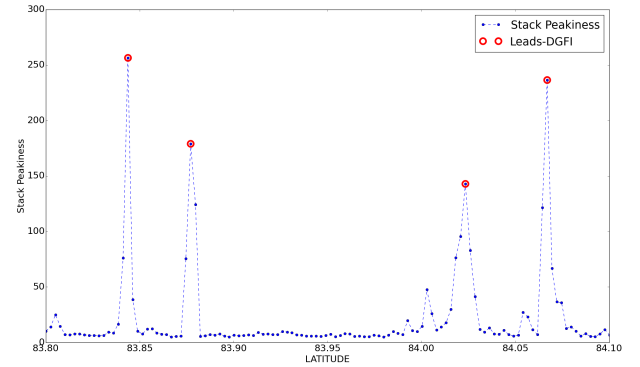


Figure 5. Stack Peakiness ( $PP_{stack}$ ) along a CryoSat-2 track flying over a sea ice region. Points classified as leads are highlighted by a red circle.

### 3. COMPARISON OF CLASSIFICATION RESULTS

After the classification a comparison is done to evaluate the quality of the open water detection for both altimetry datasets. The classification results of ENVISAT are compared with ALOS L-Band wide swath pictures with a spatial resolution of about 100 meters (Fig. 6). Leads and polynyas appear as dark areas due to the scattering properties of calm open water [9]. The altimetry-detected open-water returns are indicated by colored dots along the ENVISAT track. Fig. 6a shows an acceptable agreement between the altimetry-derived open water returns (classes 9.15.20; Fig. 6c) and the SAR image. Furthermore there is an identifiable transition from a wider to a more narrow, specular waveform type, which correlates with the increasing influence of sea ice to the measurements. However, a shift between the image and the overlaid altimetry track is detectable, which is related to different acquisition dates of the SAR image and the recorded radar pulses of ENVISAT. The area of investigation is located near the North-East coast of Greenland in the Fram Strait where fast ice-motion is frequent. For

a realistic comparison, the consideration of ice-motion with respect to the time delay between the two dataset is required. Fig. 6b, is shifted taking into account a mean ice velocity and direction by using daily ice-motion vector data of the National Snow and Ice Data Center (NSIDC). This comparison shows improved accordance between the classification results and the dark areas in the image.

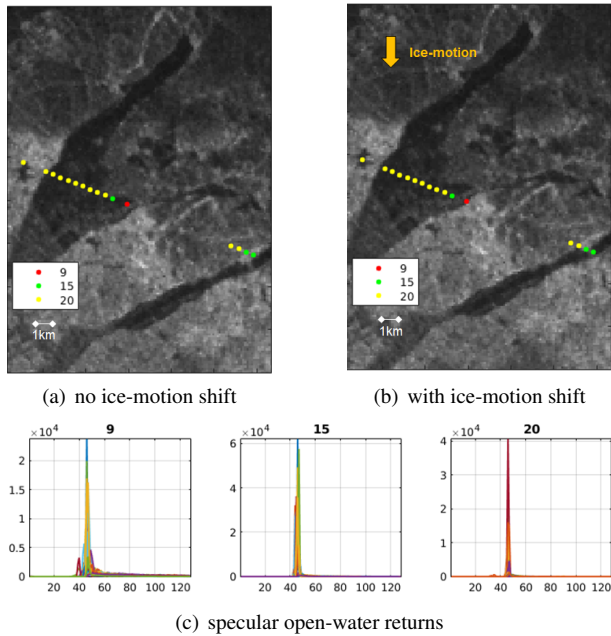


Figure 6. Comparison of ENVISAT classification result with ALOS L-Band image ©JAXA/METI 2008 (time difference 2h50min). Colored dots represent the overlain altimetry track and correspond to specular waveform classes showed in c. Waveform classes in c represent lead and polynya classes defined by very peaky and narrow waveform shapes.

Beside the comparison of the unsupervised classification result with SAR images, the lead and polynya detection results of the threshold-based classification using the CryoSat-2 RIP are also evaluated with SAR images. Therefore, Sentinel-1A images with a 40 meter spatial resolution are utilized. Figure 7 shows a detection of a small lead (cyan point). With our method, only the most peaky return in nadir is identified as lead. A detection of open water areas in off-nadir direction is avoided. The lead on the right is not identified as open water. This might be related to the fact that no measurements directly above the lead is available (no nadir lead). However, also a fine-tuning of the classification thresholds might be required. This is still under investigation.

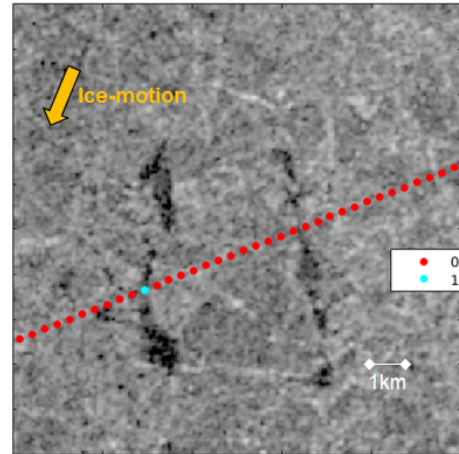


Figure 7. Comparison of CryoSat-2 classification result with Sentinel-1A C-Band image. Colored dots represent the overlain altimetry track by indicating open water returns in cyan and ice retruns in in red.

#### 4. SUMMARY

In this study, two different classification approaches, one for conventional pulse-limited altimetry data (ENVISAT) and one for Delay-Doppler data (CryoSat-2) are presented. For ENVISAT, we use an unsupervised classification of waveforms based on K-medoids and nearest-neighbor algorithms. Moreover, a threshold-based classification of CryoSat-2 surface sample stack is performed to detect open-water bodies in the arctic. The results are compared with imaging SAR data. The ice-motion within the time period between the acquisition of both data sets is taken into account. Both waveform classification approaches provide reliable results in oceanic regions affected by rapid climate change. The unsupervised classification allows a separation of different waveform and surface types without the need of training data or arbitrary threshold definition. An analysis of consecutive Delay-Doppler stacks allows for an identification of narrow leads and for an elimination of off-nadir lead returns.

#### 5. OUTLOOK

In future, a quantitative validation of the classification result is planned as well as applying the classification method to all recent and future missions (e.g., ERS-1, ERS-2 and Sentinel-3A) covering the arctic area. Therefore, it is very important to get enhanced products (e.g. instrument and stack parameters) of the present and past altimetry missions in a user-friendly data format. Furthermore, an improvement of the classification methods regarding the detection problems due to off-nadir returns is in development.

## ACKNOWLEDGEMENTS

We thank the following institutions and persons for providing the used data sets: The CryoSat-2 stack data are provided by ESA G-POD. The ENVISAT SGDR v2.1 data are provided by ESA. The JAXA/METI ALOS-1 PALSAR data (L1.5, 2008) are accessed through ASF DAAC. The Sentinel-1A data are provided by ESA and reprocessed bei Eero Rinne (Finish Meteorological Institute).

## REFERENCES

- [1] Han J., Kamber M., and Tung A. K. H. Spatial Clustering Methods in Data Mining: A Survey. *Geographic Data mining and knowledge discovery*, 2, 2001.
- [2] Duda R. O., Hart P. E., and Stork D. G. Pattern classification. *John Wiley & Sons*, 2012.
- [3] Scagliola. M. CryoSat footprints *Aresys technical note, SAR-CRY2-TEN-6331*, Aresys/ESA, Italy, 2013
- [4] Armitage T. W. K. and Davidson M. W. J. Using the interferometric capabilities of the ESA CryoSat-2 mission to improve the accuracy of sea ice freeboard retrievals. *IEEE Transactions on Geoscience and Remote Sensing*, 52(1):529–536, 2014.
- [5] Wernecke A. and Kaleschke L. Lead detection in Arctic sea ice from CryoSat-2: quality assessment, lead area fraction and width distribution. *The Cryosphere*, 9(5):1955–1968, 2015.
- [6] Ricker R., Hendricks S., Helm V., Skourup H., and Davidson M. Sensitivity of CryoSat-2 Arctic sea-ice freeboard and thickness on radar-waveform interpretation. *The Cryosphere*, 8(4):1607–1622, 2014.
- [7] Lindsay R. and Rothrock D. Arctic sea ice leads from advanced very high resolution radiometer images. *Journal of Geophysical Research*, 100(C3):4533, 1995.
- [8] Kwok R., Cunningham G. F., Wensnahan M., Rigor I., Zwally H. J., and Yi D. Thinning and volume loss of the Arctic Ocean sea ice cover: 2003-2008. *Journal of Geophysical Research: Oceans*, 114(7):2003–2008, 2009.
- [9] Dierking W. Sea ice monitoring by synthetic aperture radar. *Oceanography*, 26, June 2013.